Identification of a Musashi2 translocation as a novel oncogene in myeloid leukemia

Kyle Spinler[1,2], Michael Hamilton[1,2], Jeevisha Bajaj[1,2], Yutaka Shima[1,.2], Emily Diaz[1,2], Marcie Kritzik[1,2,3,4], and Tannishtha Reya[1,2,3,4]*

[1]Departments of Pharmacology and Medicine, University of California San Diego School of Medicine La Jolla, CA

[2]Moores Cancer Center, University of California San Diego School of Medicine, La Jolla, CA

[3]Herbert Irving Comprehensive Cancer Center, Columbia University Medical Center, New York City, NY

[4]Department of Physiology and Cellular Biophysics, Columbia University Medical Center, New York City, NY

*To whom correspondence should be addressed, t.reya@columbia.edu

ABSTRACT

Myeloid leukemias, diseases marked by aggressiveness and poor outcomes, are frequently triggered by oncogenic translocations. In the case of chronic myelogenous leukemia (CML) the BCR-ABL fusion initiates chronic phase disease with second hits allowing progression to blast crisis. Although Gleevec has been transformative for CML, blast crisis CML remains relatively drug resistant. Here we show that MSI2-HOXA9, a translocation with an unknown role in cancer, can serve as a second hit in driving bcCML. Compared to BCR-ABL, BCR-ABL/MSI2-HOXA9 led to a more aggressive disease *in vivo* with decreased latency, increased lethality and a differentiation blockade that is a hallmark of blast crisis. Domain mapping revealed that the MSI2 RNA binding domain RRM1 had a preferential impact on growth and lethality of bcCML relative to RRM2 or the HOXA9 domain. Mechanistically, MSI2-HOXA9 triggered global downstream changes with a preferential upregulation of mitochondrial components. Consistent with this, BCR-ABL/MSI2-HOXA9 cells exhibited a significant increase in mitochondrial respiration. These data suggest that MSI2-HOXA9 acts, at least in part, by increasing expression of the mitochondrial polymerase Polrmt and augmenting mitochondrial function and basal respiration in blast crisis. Collectively, our findings demonstrate for the first time that translocations involving the stem and developmental signal MSI2 can be oncogenic, and suggest that MSI, which we found to be a frequent partner for an array of translocations, could also be a driver mutation across solid cancers.

INTRODUCTION

Myeloid leukemias are a heterogeneous group of cancers, many of which have limited treatment options and are associated with poor prognosis. Chronic myeloid leukemia (CML) is characterized by the accumulation of myeloid precursors and mature myeloid cells and is driven by translocations between the BCR serine/threonine kinase gene and the ABL tyrosine kinase, resulting in a constitutively active ABL tyrosine kinase. Although imatinib mesylate effectively blocks the activity of the BCR-ABL kinase and has been used to treat CML, it is not curative because the cancer stem cells that propagate CML are no longer addicted to kinase signaling and are thus resistant to therapy[1]. Progression from CML to blast crisis CML (bcCML) occurs with acquisition of an additional oncogenic hit; this event is associated with a rapid expansion of immature blast cells and a concomitant increase in imatinib resistance such that only 50% of patients are responsive to therapy. The specific secondary translocations and mutations that have been reported in bcCML include activation of oncogenes such as RAS and MYC[2], translocations such as NUP98-HOXA9, and mutations in tumor suppressors such as RB1, TP53, and CDKN2A[3-6]. Although multiple mutations are seen in bcCML, the only mouse model of bcCML that exists was created with a combination of BCR-ABL and the NUP98/HOXA9 gene fusion (associated with t(7;11)(p15;p15)[7,8].

A new translocation between the cell fate determinant Musashi2 (MSI2) and HOXA9 was reported several years ago as a novel genetic lesion present in bcCML patients[9]. In this study, 33 CML accelerated phase/blast crisis patient samples were used for a multicolor FISH study. Among this group, 2 cases harbored a translocation, t(7;17)(p15;q23), resulting in a *MSI2/HOXA9* fusion gene. This in-frame fusion transcript retained both MSI2 RNA recognition domains and the HOXA9 homeobox domain, raising the potential for previously uncharacterized roles in CML progression. This translocation was of particular interest because it was the first reported mutation involving MSI. The MSI family of RNA binding proteins is comprised of two members, MSI1 and MSI2, each containing two RNA recognition motifs (RRMs) separated by a short linker region in the N-terminal half of the protein[10]. Functionally, MSI can either suppress translation by sequestering poly-A binding protein (PABP) or activate translation by stabilizing the RNA and recruiting the poly (A) polymerase GLD2[4] after binding to consensus sequences in the 3' untranslated region (3' UTR) of mRNA. Together, these activities result in modulation of a diverse set of genes that regulate stem and progenitor cell growth in multiple tissues including Numb, an antagonist of Notch signaling[11]. Msi2 overexpression led to elevation of the self-renewal genes *HoxA9* and *HoxA10*, the Sonic hedgehog and Notch signaling components *Gli1* and *Hes1,* and *Cyclin D1* and *Cdk2*[12]. In addition to its role in normal development[12-14], MSI proteins have emerged as critical mediators and dependencies of both solid cancers and hematologic malignancies. In pancreatic cancer, loss of MSI2 has been shown to lead to a defect in progression from PanIN to adenocarcinoma[15], exerting its impact through powerful oncogenes such as c-met and epigenetic regulators such as Brd4 and Hmgb2. In colon adenomas driven by APC loss of function mutations, MSI2 acts as an

inhibitor of known tumor suppressors including Lrig1, Bmpr1a, Cdkn1a, and Pten and sustained activation of mTORC1[16]. In context of hematologic malignancies, MSI2 is required for the development and progression of myeloid leukemias[17,18]. The loss of MSI2 reduced cancer stem cell frequency, increased differentiation, and impaired propagation of bcCML in mouse models *in vitro* and *in vivo*. Further, overexpression of an MSI2 transgene in bone marrow cells expressing BCR-ABL led to increased tumor burden[19]. MSI2 is also highly upregulated during human CML progression, and its expression serves as an early indicator of poor prognosis not only in leukemias but also in solid cancers like lung cancer[20]. However, while these studies have collectively identified MSI genes as clear dependencies in cancers and have highlighted their potential utility as a prognostic, whether naturally occurring MSI translocations and mutations can serve as oncogenes in driving cancer growth remains unknown.

Here we have used the MSI2-HOXA9 fusion gene to show that this translocation, found in patients with bcCML, can cooperate with BCR-ABL to drive progression to bcCML, demonstrating for the first time that the MSI gene alterations that occur in patients can serve as oncogenes. Further, the MSI2 RNA recognition motifs (RRMs) were essential to the oncogenicity of this translocation and they act to control bcCML by enhancing mitochondrial energetics. Deletion of the RRM1 abrogated the enhanced cell growth conferred by the MSI2-HOXA9 fusion *in vitro* and *in vivo*. Additionally, the MSI2-HOXA9 fusion resulted in cells that showed a rise in maximum mitochondrial respiration rate likely due to the concomitant increase in the mitochondrial polymerase, Polrmt, whose elevated expression may be driven by the abnormal localization of MSI2-HOXA9 to the cell nucleus. In all, these data demonstrate a novel MSI2-translocation driven downstream event that leads to a more energetic, differentiation arrested aggressive state thus triggering CML progression to bcCML.

RESULTS

MSI2-HOXA9 confers a growth advantage and arrests differentiation

To test the oncogenic activity of the MSI2-HOXA9 fusion, we generated an MSI2-HOXA9 gene reflecting the breakpoint reported in CML patients (t(7:17)(p15;q23)). Specifically, we fused the amino terminus of MSI2 (containing both RNA binding domains (RRMs)) with the carboxyl terminus of the HOXA9 protein (containing the homeobox domain) (Fig. 1A). We infected murine hematopoietic stem/progenitor (ckit+, Lineage-, Sca1+ (KLS)) cells with viruses encoding BCR-ABL together with either MSI2-HOXA9 or an empty vector and tested their colony forming ability (Fig. 1B). Compared to BCR-ABL and empty vector (hereafter referred to as just BCR-ABL), the combination of BCR-ABL and MSI2-HOXA9 infected cells exhibited significantly increased colony formation in primary (Fig. 1C) and secondary plating (Fig. 1D).

To test whether the MSI2-HOXA9 fusion confers a growth advantage *in vivo*, we transplanted hematopoietic stem and progenitor cells infected with BCR-ABL and MSI2-HOXA9 or an empty vector into lethally

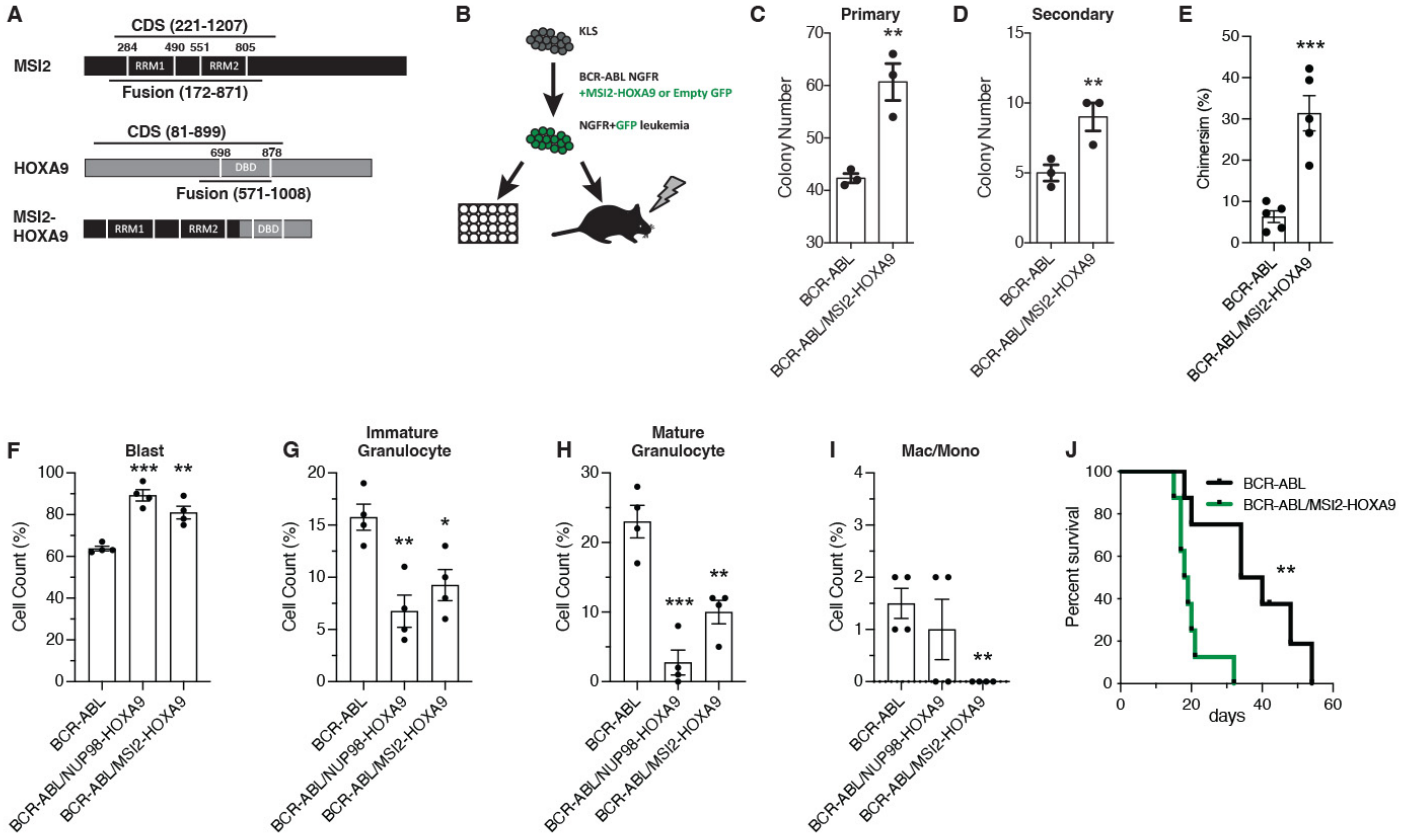

Figure 1. MSI2-HOXA9 expression leads to cancer cell growth advantage and differentiation arrest

(*A*) Schematic of the MSI2-HOXA9 fusion protein. The fusion retains both MSI2 RNA binding domains and the HOXA9 DNA binding domain. (*B*) Experimental design for *in vitro* colony assay or *in vivo* transplantation of BCR-ABL/Control or BCR-ABL/MSI2-HOXA9 expressing KLS cells. Transplanted mice were subsequently assessed for chimerism, survival, and cancer cell differentiation. (*C*) Primary colony assay of BCR-ABL/Control or BCR-ABL/MSI2-HOXA9 expressing KLS cells. **P=0.007 (n=3 technical replicates). (*D*) Secondary colony assay of BCR-ABL/Control or BCR-ABL/MSI2-HOXA9 expressing KLS cells. **P=0.009 (n=3 technical replicates). (*E*) Chimerism of BCR-ABL/Control or BCR-ABL/MSI2-HOXA9 transplanted cells at 13 days. ***P=0.0005 (n=5 mice per group). (*F-I*) Lin- BCR-ABL/Control, BCR-ABL/NUP98-HOXA9, or BCR-ABL/MSI2-HOXA9 expressing cells were sorted from primary transplants and used to generate cytospins that were then stained with Giemsa and May-Grunwald stains (n=4 mice per group). (*F*) Quantification of blast cells. **P=0.001, ***P=0.0001 (n=4 mice per group). (*G*) Quantification of immature granulocytes. *P=0.01, **P=0.004. (*H*) Quantification of mature granulocytes. **P=0.004, ***P=0.0005. (*I*) Quantification of differentiated macrophages and monocytes. **P=0.002. (*J*) Survival of mice transplanted with BCR-ABL/Control or BCR-ABL/MSI2-HOXA9 expressing KLS cells. **P=0.002. Two-tailed unpaired Student's t-tests were used to determine statistical significance.

irradiated recipient mice and monitored disease development over time (Fig. 1B). Animals transplanted with cells harboring both BCR-ABL and MSI2-HOXA9 exhibited far more aggressive disease with a ~3-fold increase in chimerism relative to the cohort receiving cells carrying BCR-ABL alone (Fig. 1E). To determine whether disease observed with BCR-ABL and MSI2-HOXA9 was more aggressive because it was more undifferentiated than disease driven by BCR-ABL alone, we compared the BCR-ABL/MSI2-HOXA9 leukemic cells to the previously established model of blast crisis CML driven by BCR-ABL/NUP98-HOXA9 (Dash et al. 2002). To this end, we transplanted mice with KLS cells infected with either BCR-ABL, BCR-ABL/NUP98-HOXA9, or BCR-ABL/MSI2-HOXA9 and sorted Lin- leukemia cells from these mice. Even though Lin- cells were compared, which are generally more undifferentiated, based on Giemsa staining BCR-ABL/MSI2-HOXA9 cells displayed an increase in less differentiated blasts (82% vs. 61%) and a concomitant decrease in more differentiated cells compared to BCR-ABL-driven disease and, in this regard, was most consistent with the previously described bcCML model (Fig. 1F-I, Fig. S1A-C). Additionally, by FACS total Lin- content was also increased in BCR-ABL/MSI2-HOXA9 relative to BCR-ABL alone (57% vs. 16%, Fig. S1D). The change in differentiation state driven by MSI2-HOXA9 cells suggested that when coupled with BCR-ABL, MSI2-HOXA9 can drive chronic phase CML to blast crisis, and thus serve as an oncogene.

Reflecting the development of this more aggressive disease, mice transplanted with BCR-ABL/MSI2-HOXA9 infected cells displayed significantly reduced survival. Thus, while the median survival of mice carrying BCR-ABL alone was 37 days, that of the BCR-ABL/MSI2-HOXA9 group was just 18 days, an 8-fold increase in the risk of death (HR=0.11) (Fig. 1J). Collectively, these findings indicate that the MSI2/HOXA9 fusion protein has oncogenic activity and can cooperate with BCR-ABL to drive cancer progression.

MSI2 RNA binding domains play a key role in BCR-ABL/MSI2-HOXA9-driven oncogenesis

Given that MSI2 and HOXA9 both play key roles in regulation of gene expression – MSI2 as an RNA binding protein and HOXA9 as a homeodomain transcription factor – we tested whether the oncogenic ability of MSI2-HOXA9 was dependent on the RNA binding domains of MSI2 (RRM1 and RRM2) or on the DNA binding domain (DBD) of HOXA9. We generated MSI2-HOXA9 domain mutants lacking either RRM1 or RRM2 as well as a truncated mutant lacking the HOXA9 DNA binding domain (Fig. 2A). To test whether the domain mutants would blunt the growth advantage provided by MSI2-HOXA9 in the presence of BCR-ABL, we infected KLS cells with viruses encoding BCR-ABL and either full length MSI2-HOXA9 or the domain mutants and performed colony assays. The loss of either RRM1 or RRM2 led to a significant loss in colony forming ability compared to cells infected with BCR-ABL/MSI2-HOXA9 (>2-fold for both ΔRRM1 and ΔRRM2), indicating that each RNA binding domain was required for MSI2-HOXA9 activity (Fig. 2B). While loss of the HOXA9 domain did not significantly impact primary colony formation, some impact (1.7-fold

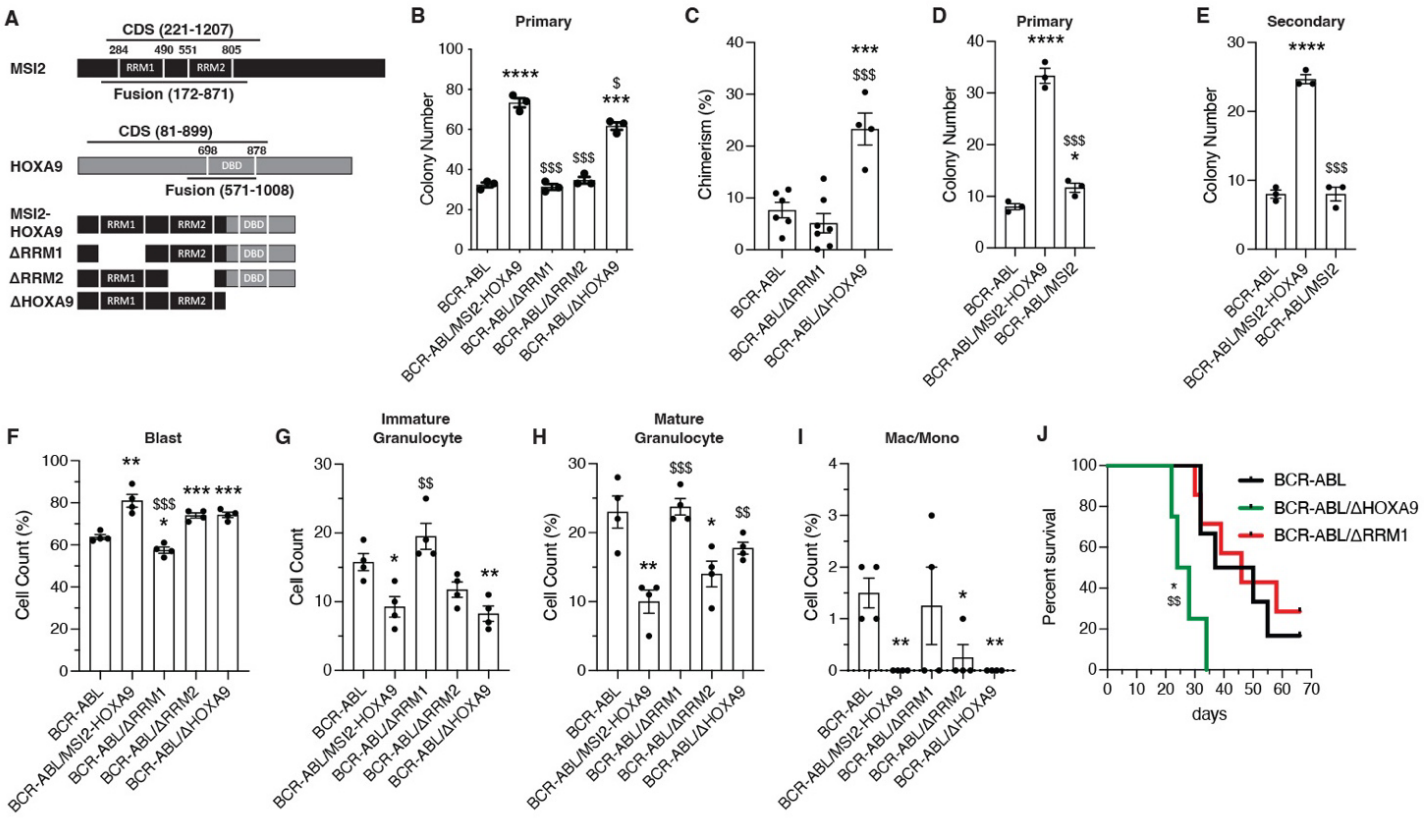

Figure 2. BCR-ABL/MSI2-HOXA9 cell growth and differentiation is dependent on MSI2 RRM1

(*A*) Schematic of MSI2-HOXA9 fusion protein and mutant versions generated to test domain dependencies. ΔRRM1 and ΔRRM2 are deletions of the MSI2 RNA binding domains 1 and 2 respectively, while ΔHOXA9 introduces a stop codon at the break point to eliminate the HOXA9 DNA binding domain. (*B*) Primary colony formation of KLS cells expressing BCR-ABL/Control or BCR-ABL + variations of the MSI2-HOXA9 fusion protein. *=significance from BCR-ABL/Control, ***P=0.0002, ****P<0.0001; $=significance from BCR-ABL/MSI2-HOXA9, $P=0.01, $$$P=0.0001 for ΔRRM1, $$$P=0.0002 for ΔRRM2 (n=3 technical replicates). (*C*) Chimerism of BCR-ABL/Control, BCR-ABL/ΔRRM1, or BCR-ABL/ΔHOXA9 cells 14 days post-transplantation. ***P=0.0009 significance from BCR-ABL/Control, $$$P=0.0004 significance from BCR-ABL/ΔRRM1 (n=6 mice for BCR-ABL/Control, n=7 for BCR-ABL/ΔRRM1, n=4 for BCR-ABL/ΔHOXA9). (*D*) Primary colony formation of KLS cells expressing BCR-ABL/Control or BCR-ABL + MSI2-HOXA9 fusion protein or full length wild-type MSI2. *=significance from BCR-ABL/Control, *P=0.02, ****P<0.0001; $=significance from BCR-ABL/MSI2-HOXA9, $$$P=0.0002 (n=3 technical replicates). (*E*) Secondary colony formation of KLS cells expressing BCR-ABL/Control or BCR-ABL + MSI2-HOXA9 fusion protein or full length wild-type MSI2. *=significance from BCR-ABL/Control, ****P<0.0001; $=significance from BCR-ABL/MSI2-HOXA9, $$$P=0.0002 (n=3 technical replicates). (*F-I*) Lin- BCR-ABL/Control or BCR-ABL + variations of the MSI2-HOXA9 fusion protein were sorted from primary transplants and used to generate cytospins that were then stained with Giemsa and May-Grunwald stains. *=significance from BCR-ABL/Control, $=significance from BCR-ABL/MSI2-HOXA9 (n=4 mice per group). (*F*) Quantification of blast cells. *P=0.01, **P=0.001, ***P=0.0008, $$$P=0.0004. (*G*) Quantification of immature granulocytes. *P=0.01, **P=0.004, $$P=0.005. (*H*) Quantification of mature granulocytes. *P=0.02, **P=0.004, $$P=0.006, $$$P=0.0005. (*I*) Quantification of differentiated macrophages and monocytes. *P=0.01, **P=0.002. (*J*) Survival of mice transplanted with BCR-ABL/Control, BCR-ABL/ΔRRM1, or BCR-ABL/ΔHOXA9 expressing KLS cells. *P=0.01 significance from BCR-ABL/Control, $$P=0.007 significance from BCR-ABL/ΔRRM1. Two-tailed unpaired Student's t-tests were used to determine statistical significance.

reduction) was seen at secondary plating (Fig. S1E). These data suggest that the domains could be differentially important, with the RRMs having a dominant impact on bcCML growth. Consistent with the impact on growth *in vitro*, transplantation of BCR-ABL/ΔRRM1 blunted leukemic growth *in vivo* while loss of the HOXA9 portion of the MSI2-HOXA9 fusion did not impact chimerism compared to BCR-ABL/MSI2-HOXA9 (~30% for MSI2-HOXA9, ~25% for ΔHOXA9, ~7% for ΔRRM1; Fig. 2C and compare to Fig. 1E). Although each RRM was necessary for bcCML growth, expression of full length wild-type MSI2 did not impart any growth advantage when combined with BCR-ABL in either primary (Fig. 2D) or secondary colony assays (Fig. 2E) relative to BCR-ABL alone. The fact that the 5' portion of MSI2 but not the full-length protein is oncogenic suggests that the 3' end may regulate or mask MSI2 oncogenic activity, consistent with the highly regulated activity of wild type MSI2 proteins during development and in stem cell maintenance. Whether this regulatory effect is due to altered binding activity resulting from a change in MSI2 protein conformation, a shift in cellular localization relative to wild type MSI2, or through some other mechanism is not clear and represents an important question for future study.

We also tested which domains may be important for driving the more undifferentiated state created by MSI2-HOXA9. Analysis of established primary cancer cells stained with Giemsa and May-Grunwald stains indicated that while both RRM1 and RRM2 similarly impacted growth in colony assays (78 colonies for MSI2-HOXA9, ~35 colonies for both ΔRRM1 and ΔRRM2; Fig. 2B, Fig. S1E), only deletion of RRM1 impacted differentiation (Fig. 2F-I, Fig. S1F-H), leading to a reduction in blast cell counts (~80% for MSI2-HOXA9, 60% for BCR-ABL only, 58% for ΔRRM1; Fig. 2F) and an increase in differentiated myeloid cells (Fig. 2G-I), and resulting in a disease similar in composition to that driven by BCR-ABL alone.

Between the two MSI2 RRMs, the data above suggested that RRM1 is more critical than RRM2. This is consistent with RRM1 having been shown to provide most of the specificity and higher binding energy relative to RRM2[21], and thus we focused on RRM1 deletion for subsequent *in vivo* investigation. Further, supporting the observation that the MSI2 RRM1 is critical for growth and differentiation, the deletion of RRM1 led to significantly longer survival that was no different from the survival of mice transplanted with BCR-ABL alone (P=0.97) (Fig. 2J). Thus, while the median survival of mice with leukemia driven by BCR-ABL/ΔHOXA9 was 26 days, the loss of RRM1 (BCR-ABL/ΔRRM1) was 46 days, similar to BCR-ABL alone (43.5 days). This resulted in a 12-fold (HR=0.08) increase in risk of death for BCR-ABL/ΔHOXA9 compared to BCR-ABL only and a 15-fold (HE=0.06) increase in risk of death for BCR-ABL/ΔHOXA9 compared to BCR-ABL/ΔRRM1. Together, these results demonstrate that the MSI2 RRM1 is critical for the lethality seen in BCR-ABL/MSI2-HOXA9 bcCML.

MSI2-HOXA9- triggers global changes in transcriptional programs

To understand how the MSI2-HOXA9 translocation promotes bcCML, we compared gene expression patterns in BCR-ABL and BCR-ABL/MSI2-HOXA9-driven disease. RNA-seq analysis was carried out on lineage negative cells from leukemia established with BCR-ABL or BCR-ABL/MSI2-HOXA9 (Fig. 3A, Fig. S2A). Network mapping of all differentially expressed genes (q-value <0.05) using non-redundant functional grouping revealed an enrichment of metabolic processes with oncogenic pathways and developmental programs (Fig. 3B). Programs that were dominantly upregulated by MSI2/HOXA9 were those involved in development, including Aldh1a1, Erbb3, and Kit, consistent with BCR-ABL/MSI2-HOXA9 driving a more undifferentiated disease (Fig. 3C), known oncogenes, including Frat1, Map7, and Fzd3 (Fig. 3D), and components of the mitochondria including mt-Co2, mt-Atp8, and mt-Nd5 (Fig. 3E). Gene set enrichment analysis suggested an enrichment in genes associated with the mitochondrial transcription pathway (p-value <0.05) (Fig. 3F); this finding was subsequently confirmed by qRT-PCR (Fig. 3G). The impact on mitochondrial gene expression was unexpected and we thus pursued this to gain insight into whether BCR-ABL/MSI2-HOXA9-driven mitochondrial changes may be pivotal in driving leukemia growth.

Among the genes most enriched in BCR-ABL/MSI2-HOXA9-driven bcCML were key components of the mitochondrial respiratory chain, including Complex I, Complex III, Complex IV and the F0 subunit of ATP synthase (mt-Atp6 and mt-Atp8). Analysis of metabolic capacity and mitochondrial function on Lin- bcCML using the Seahorse Cell Mito Stress Test (Fig. 4A) revealed that MSI2-HOXA9 significantly increased basal respiration (Fig. 4B, C), ATP production (Fig. 4D), and maximal respiration (Fig. 4E). These three findings suggest that introduction of MSI2-HOXA9 results in a cell operating at a higher energetic level. In contrast, most of the other mitochondrial parameters we evaluated were not significantly impacted (Fig. S2B-E). Further, BCR-ABL/MSI2-HOXA9 increased basal glycolysis (Fig. 4F, G), glycolytic reserves (Fig. 4H), and maximum glycolysis (Fig. 4I). Again, these data suggest that in addition to requiring a higher basal energy level, they also exhibit greater maximal energy capacity. We also observed an increase in the lactate output to glucose uptake ratio in BCR-ABL/MSI2-HOXA9 cells compared to BCR-ABL cells *in vitro* (Fig. S2F-H) suggesting greater energy demands in these cells. A plot of the basal oxygen consumption rate (OCR) against extracellular acidification rate (ECAR) revealed a cellular energetics landscape wherein BCR-ABL/MSI2-HOXA9 cells are characteristically more energetic than BCR-ABL cells (Fig. 4J). Finally, OCR data showed that BCR-ABL/MSI2-HOXA9 cells operate in a more energetically optimal way; their mitochondria were in a state close to 3.5 (Fig. 4K), with state 3 being the theoretical maximal respiration state[22]. Collectively, these findings suggest that MSI2-HOXA9 exerts its effects at least in part by augmenting mitochondrial function and basal respiration in leukemia cells.

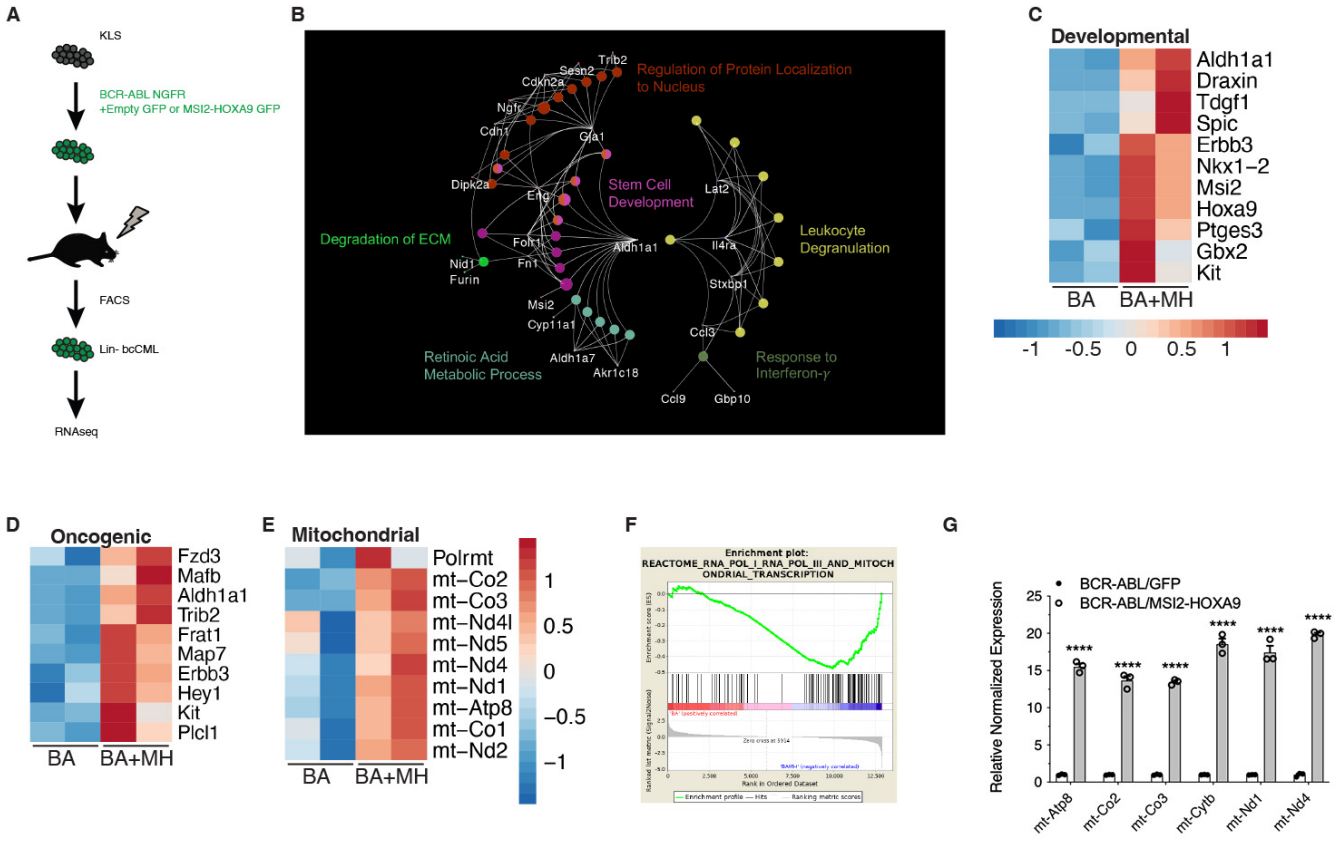

Figure 3. MSI2-HOXA9 regulates gene expression including mitochondrial, developmental, and oncogenic genes

(*A*) Schematic of RNAseq workflow. (*B*) Network map of differential genes from RNAseq of Lin- BCR-ABL/Control vs. Lin- BCR-ABL/MSI2-HOXA9. (*C*) Heatmap of developmental genes from RNAseq of Lin- BCR-ABL/Control vs. Lin- BCR-ABL/MSI2-HOXA9. (*D*) Heatmap of oncogenic genes from RNAseq of Lin- BCR-ABL/Control vs. Lin- BCR-ABL/MSI2-HOXA9. (*E*) Heatmap of mitochondrial genes from RNAseq of Lin- BCR-ABL/Control vs. Lin- BCR-ABL/MSI2-HOXA9. (*F*) Gene Set Enrichment Analysis plot of mitochondrial transcription program generated from RNAseq of Lin- BCR-ABL/Control vs. Lin- BCR-ABL/MSI2-HOXA9. (*G*) Validation of selected mitochondrial genes upregulated in Lin- BCR-ABL/MSI2-HOXA9 relative to Lin- BCR-ABL/Control. ****P<0.0001. Two-tailed unpaired Student's t-tests were used to determine statistical significance.

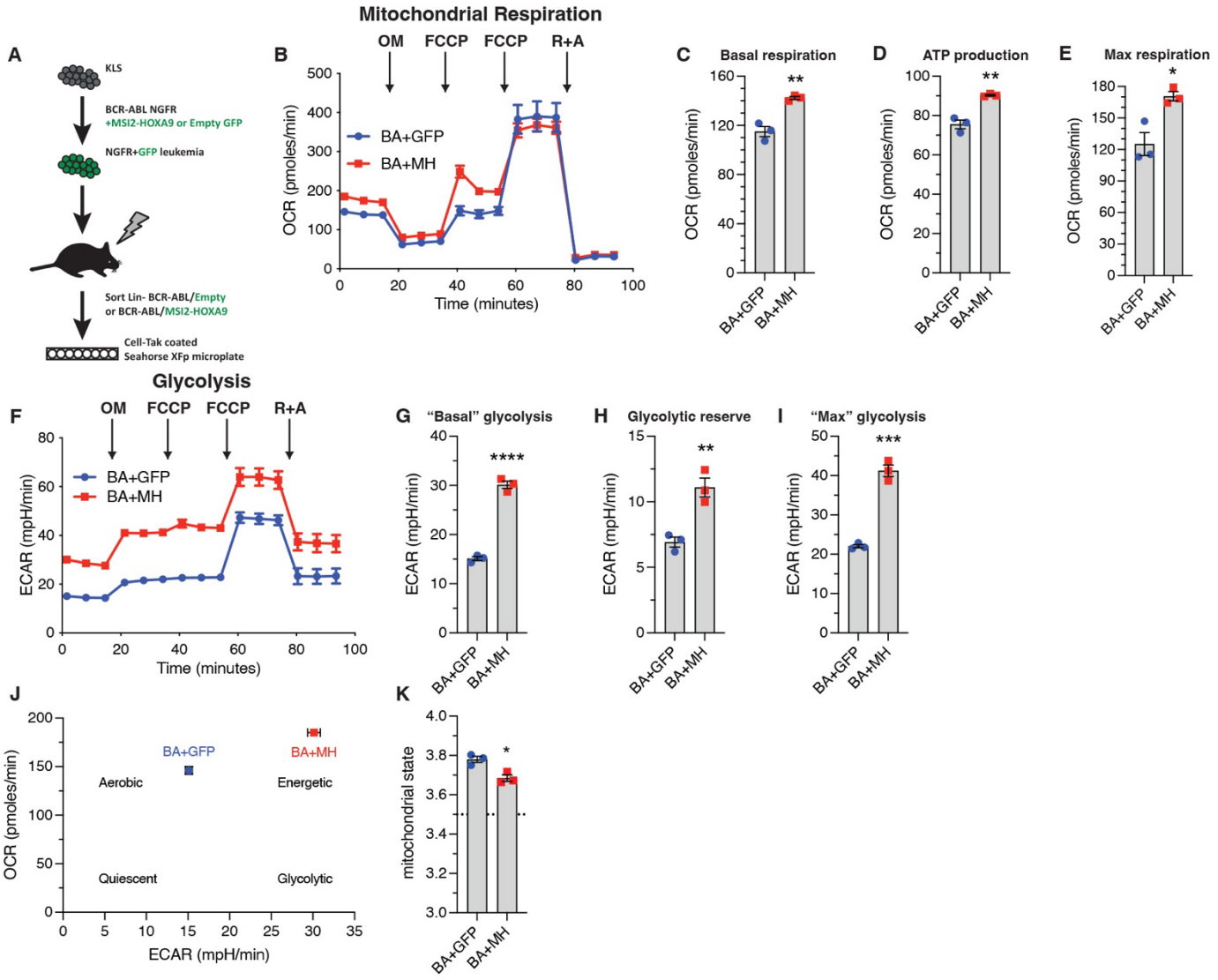

Figure 4. Elevated mitochondria gene expression leads to increased cellular respiration and energetics

(*A*) Schematic of experimental workflow to assess Lin- BCR-ABL/Control vs. Lin- BCR-ABL/MSI2-HOXA9 cancer cell energetics using the Seahorse XFp Cell Mito Stress Test Kit. (*B*) Oxygen consumption rate (OCR) of Lin- BCR-ABL/Control and Lin- BCR-ABL/MSI2-HOXA9 to measure mitochondrial respiration (n=3 technical replicates for each cell type). (*C*) Basal respiration rate of Lin- BCR-ABL/Control and Lin- BCR-ABL/MSI2-HOXA9 determined from the OCR trace. **P=0.003. (*D*) ATP production rate of Lin- BCR-ABL/Control and Lin- BCR-ABL/MSI2-HOXA9 determined from the OCR trace. **P=0.002. (*E*) Maximum respiration rate of Lin- BCR-ABL/Control and Lin- BCR-ABL/MSI2-HOXA9 determined from the OCR trace after the first FCCP injection. *P=0.01. (*F*) Extracellular acidification rate (ECAR) of Lin- BCR-ABL/Control and Lin- BCR-ABL/MSI2-HOXA9 to measure glycolysis (n=3 technical replicates for each cell type). (*G*) "Basal" glycolysis of Lin- BCR-ABL/Control and Lin- BCR-ABL/MSI2-HOXA9 determined from the ECAR trace, ****P<0.0001. (*H*) Glycolytic reserve of Lin- BCR-ABL/Control and Lin- BCR-ABL/MSI2-HOXA9 determined from the ECAR trace, **P=0.006. (*I*) "Maximum" glycolysis of Lin- BCR-ABL/Control and Lin- BCR-ABL/MSI2-HOXA9 determined from the ECAR trace, ***P=0.0002. (*J*) Energetic landscape of Lin- BCR-ABL/Control and Lin- BCR-ABL/MSI2-HOXA9 generated by plotting the basal OCR vs. basal ECAR for each cell type. (*K*) Mitochondrial state determined from OCR data. *P=0.01. Two-tailed unpaired Student's t-tests were used to determine statistical significance.

MSI2-HOXA9 impacts mitochondrial gene expression through control of the mitochondrial polymerase, Polrmt

To understand the basis of the alteration in mitochondrial gene expression in BCR-ABL/MSI2-HOXA9 leukemia and the concomitant increase in energy production, we tested whether MSI2-HOXA9 impacted mitochondrial gene expression directly in the mitochondria or indirectly through control of the polymerase and/or transcription factors. We thus assessed expression of the mitochondrial polymerase and selected mitochondrial transcription factors and found a 5-fold increase in expression of the lone mitochondrial polymerase (Polrmt) in BCR-ABL/MSI2-HOXA9 cells as well as significant increases in the transcription initiation factor Tfb2m and the mitochondrial transcription factor regulator Nrf1, 1.5-fold and 1.4-fold, respectively (Fig. 5A). While Tfb2m and Nrf showed a significant increase in expression, we chose to focus on the much greater impact seen on Polrmt expression. Since these components are transcribed in the nucleus, the data suggest that MSI2-HOXA9 controls mitochondrial gene expression by promoting expression of Polrmt and key transcription factors. Consistent with this, MSI2-HOXA9 was preferentially found in the nucleus relative to MSI2 (Fig. 5B-D). Further, we identified 10 occurrences of the minimal MSI2 RRM1 consensus binding sequence UAGU within the Polmrt transcript. These data suggest a model in which MSI2-HOXA9 localizes to the nucleus and elevates Polrmt expression. Polrmt and the mitochondrial transcription factors in turn control expression of mitochondrial genes that encode the components of the respiratory chain, leading to increased mitochondrial function and cellular energetics that drive the aggressiveness of bcCML (Fig. 5E).

DISCUSSION

The stem cell gene MSI2 is often hijacked and aberrantly upregulated in cancer, where it can drive sustained self-renewal of cancer stem cells, leading to tumor growth, therapy resistance, and disease progression. Although MSI2 was shown to be a dependency of aggressive myeloid leukemias as well as solid cancers such as pancreatic cancer[15,17-19], and its transgenic overexpression can lead to increased tumor burden[19], whether MSI2 translocations or mutations harbored in patients can serve as oncogenes and driver mutations was unknown. Because a translocation between MSI2 and HOXA9 had been reported to occur in blast crisis CML patients, we focused on testing whether this translocation could be an oncogene in myeloid leukemia. Our data presented here show that overexpression of the MSI2-HOXA9 allele together with BCR-ABL can trigger the development of blast crisis CML. These findings are important in that they represent the first demonstration that an aberrant MSI2 genetic lesion found in patients can be oncogenic.

The new bcCML mouse model we developed is a valuable resource to the field, particularly because there is only one other model for bcCML[7] developed over 20 years ago. bcCML is an aggressive, highly lethal malignancy, and new models are critical to better understand the biology of the disease, identify molecular

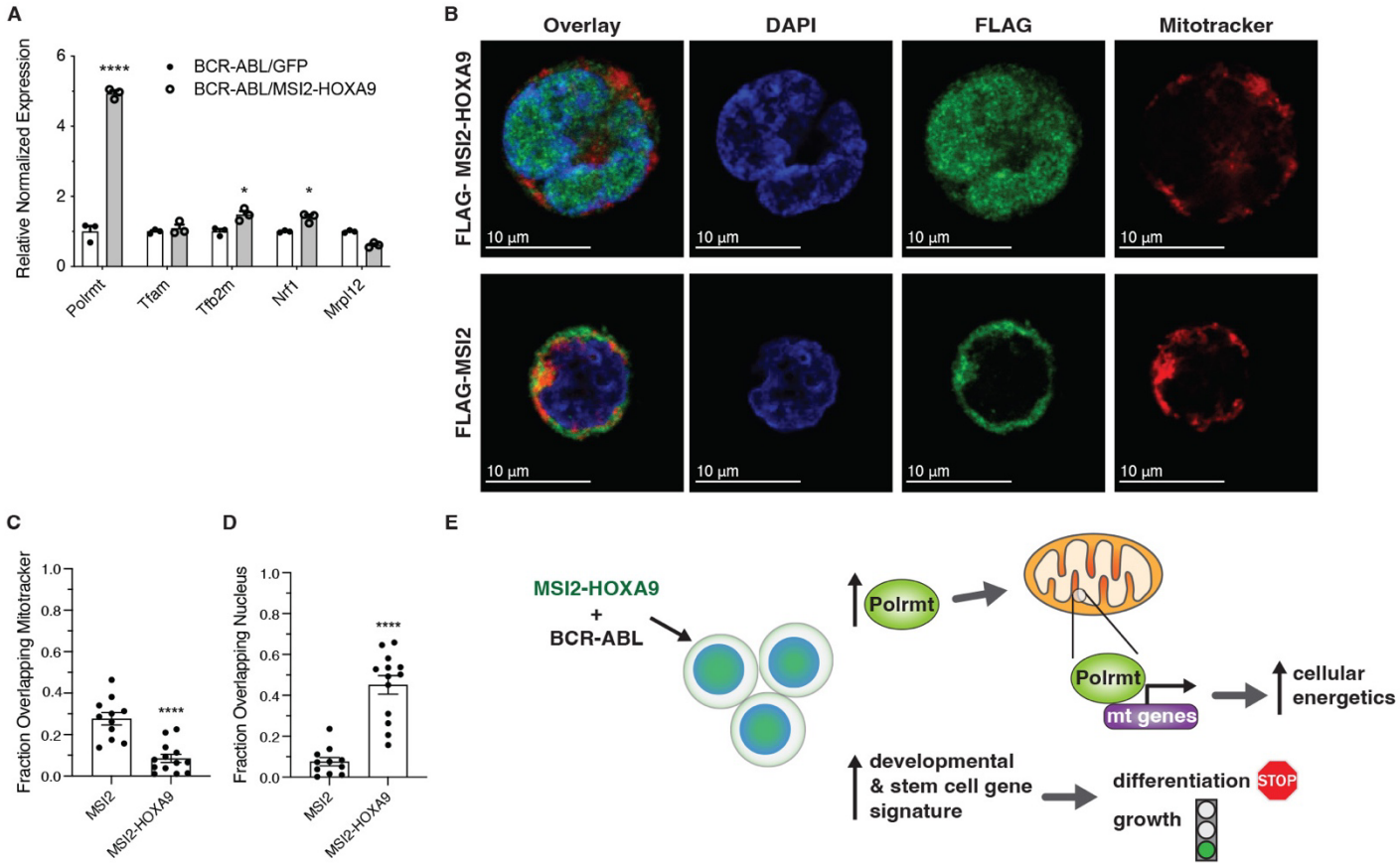

Figure 5. MSI2-HOXA9 localizes to the nucleus and increases Polrmt expression

(*A*) qRT-PCR of genes directly involved in regulation of mitochondrial gene expression. *P=0.02 for Tfb2m, *P=0.01 for Nrf1, ****P<0.0001 for Polrmt. (*B*) Representative immunofluorescent images of K562 cells expressing Flag-tagged MSI2 or Flag-tagged MSI2-HOXA9 (scale bar=10µm). (DAPI= blue, FLAG-MSI2 or FLAG-MSI2-HOXA9= green, mitotracker= red). (*C*) Overlap of Flag-tagged MSI2 or MSI2-HOXA9 with mitochondria. ****P<0.0001 (n=11 for MSI2, n=13 for MSI2-HOXA9). (*D*) Overlap of Flag-tagged MSI2 or MSI2-HOXA9 with the nucleus. ****P<0.0001 (n=11 for MSI2, n=13 for MSI2-HOXA9). (*E*) Proposed mechanism by which the MSI2-HOXA9 fusion protein promotes an undifferentiated aggressive cancer cell. Two-tailed unpaired Student's t-tests were used to determine statistical significance.

dependencies, and test new approaches to therapy. The MSI2-HOXA9/BCR-ABL mouse model is characterized by a shift in cellular composition during disease progression, with an increase in blast cells and a decrease in more differentiated blood cells. This is consistent with the human disease as well as with the existing NUP98-HOXA9/BCR-ABL mouse model. Importantly, comparison of MSI2-HOXA9 and NUP98-HOXA9-driven leukemias may reveal activation of shared as well as unique programs. Analysis in each case is valuable: identification of common pathways activated in the two models may reveal underlying programs that are fundamental to blast crisis CML growth, regardless of driver gene, while identification of unique pathways may provide key insight into mechanisms of initiation and identify oncogene-specific dependencies. Overall, the MSI2-HOXA9 leukemia model we developed will contribute to a deeper understanding of how a benign, chronic disease transitions to an aggressive, highly lethal disease, and may reveal new vulnerabilities that can be targeted to stop this deadly progression.

Domain mutants of the MSI2-HOXA9 protein allowed us to better delineate the contributions of the two RRM domains and the DBD domain of HOXA9. Deletion of the MSI2 RRM1 reduced the oncogenicity of the MSI2-HOXA9 fusion *in vitro* and *in vivo*, resulting in a disease similar to BCR-ABL alone as chimerism and survival were similar to the CML model. RRM1 deletion prevented the increase in blast cells that the full fusion produced and resulted in a composition of differentiated cells and blasts similar to BCR-ABL. While the loss of the HOXA9 portion of the MSI2-HOXA9 had some impact in secondary plating *in vitro*, loss of the DBD did not impact survival and progression of bcCML *in vivo*. These data identify the RRM1 domain of the new allele as the predominant driver of MSI-HOXA9's oncogenic capacity.

To understand the downstream mechanism by which MSI2-HOXA9 cooperated with BCR-ABL to drive CML into blast crisis, we analyzed the transcriptomic changes triggered by MSI2-HOXA9 in the context of BCR-ABL expression. Among the global changes in gene expression patterns observed, the most highly enriched factors were developmental and stem cell signals such Aldh1a1, Erbb3, and Kit, consistent with the undifferentiated nature of blast crisis CML that was driven by MSI2-HOXA9. In addition, there was a striking increase in the expression of mitochondrial genes, with many critical components of the respiratory chain significantly elevated. This translated to increased mitochondrial activity as well as an increase in basal respiration and cellular energetics. Among the genes regulated through MSI2-HOXA9 activity was Polrmt, the sole RNA polymerase that controls mitochondrial gene expression. Our data suggest that dysregulated Polrmt activity upregulates the expression of key respiratory chain proteins, increasing mitochondrial function and helping to fuel uncontrolled growth of the leukemia. While the increased mitochondrial energetics may be related to the increased proliferation that is also a hallmark of bcCML, several studies have suggested a link between mitochondrial activity and leukemia cell differentiation as well. For example, Yehudai et al showed that blocking mitochondrial DNA replication using either genetic knockdown or chemical inhibitors promotes

the differentiation of human AML cells[23]. Further, in a study examining the relationship between microvesicle-driven release of mitochondria, energy metabolism, and leukemia cell differentiation, Zhao et al showed that disrupting the release of mitochondria or blocking mitochondrial function significantly impacts the differentiation of human leukemia cell lines[24]. The possibility that a fundamental relationship exists between mitochondrial pathways and the differentiation state of aggressive leukemias is exciting and may reveal new strategies for therapy. The contribution of mitochondrial activity to proliferation versus differentiation will be an important question to address in future work.

While the main focus of the work reported here is the role of MSI2 translocation in hematologic malignancies, this discovery may lay a foundation for defining the role MSI2 genetic lesions may play as oncogenes in other disease settings. Not only have other MSI2 fusions been detected in patient leukemia samples (i.e., PAX5-MSI2[25], EVI1-MSI2[26], TTC40-MSI2[27]), but we have found that MSI2 is also a frequent partner for an array of translocations in solid cancers including breast, lung and colon cancer[28] (Supplementary Table 1). This suggests that MSI2 could be functioning as an oncogene in human disease in multiple other contexts, and with multiple other partners. Thus, our work demonstrating that MSI2 translocations can be oncogenic in context of bcCML may provide a paradigm for understanding how dysregulation of this pathway may be oncogenic in a wider array of cancers.

MATERIALS AND METHODS

Mice

All animal experiments were performed according to protocols approved by the University of California San Diego Institutional Animal Care and Use Committee. Mice were bred and maintained in the animal care facilities at the University of California San Diego. The following mice were used: B6-CD45.2 and B6-CD45.1 (Strain: B6.SJL-Ptprc^{a}Pepc^{b}/BoyJ); NSG mice (Strain: NOD.Cg-Prkdc^{scid} Il2rg^{tm1Wjl}/SzJ). All mice were 8-16 weeks of age.

Generation and Analysis of Leukemic Mice

For BCR-ABL1/NUP98-HOXA9-driven blast crisis CML (bcCML), BCR-ABL-driven CML, or BCR-ABL/MSI2-HOXA9, bone marrow-derived KLS cells were isolated and sorted from CD45.2 B6 mice. All sorted cells were cultured overnight in X-Vivo15 media (Lonza) supplemented with 50 μM 2-mercaptoethanol, 10% (vol/vol) fetal bovine serum (FBS), 1% penicillin-streptomycin, SCF (100 ng/ml, R&D Systems) and TPO (20 ng/ml, R&D Systems). Cells were retrovirally infected with MSCV-BCR-ABL-IRES-NGFR and MSCV-NUP98-HOXA9-IRES-huCD2 to generate bcCML; MSCV-BCR-ABL-IRES-NGFR and MSCV-EMPTY-IRES-GFP to generate CML; MSCV-BCR-ABL-IRES-NGFR and MSCV-MSI2-HOXA9-IRES-GFP to generate BCR-ABL/MSI2-HOXA9 leukemia. Subsequently, cells were harvested 48 hours after

infection. For primary transplants, infected and sorted cells were transplanted retro-orbitally into cohorts of sub-lethally (6 Gy) irradiated CD45.1 mice. Disease mice were analyzed as previously described[29].

In Vitro Methylcellulose Colony Formation Assay

For primary plating, KLS cells isolated from B6-CD45.2 mice were infected as described above, incubated in the presence of virus for 48 hours, and then sorted for oncogene tags (NGFR and GFP). 250 cells were plated in triplicate in cytokine-free methylcellulose media (Methocult GM M3234, StemCell Technologies) supplemented with 20 ng/mL IL-3 and 20 ng/mL SCF (R&D Systems), 2% FBS, and 1% penicillin-streptomycin. For secondary plating, primary plates were dissociated, replicates were combined and cells were collected and washed in PBS. 2500 cells were re-plated in fresh methylcellulose media and cytokines.

Cell Isolation and FACS Analysis

Cells were suspended in Hanks' balanced salt solution (HBSS) (Gibco, Life Technologies) containing 5% (vol/vol) fetal bovine serum and 2 mM EDTA and prepared for FACS analysis and sorting as previously described[30]. Red blood cells were lysed using RBC Lysis Buffer (eBioscience) before and antibody incubation. For KLS isolation cells were incubated with CD117 (ckit) magnetic beads (Miltenyi Biotec) followed by positive selection using a AutomacsPro (Miltenyi Biotec). Following ckit enrichment, cells were incubated with 2B8 (ckit), D7 (Sca1) and the following antibodies to define lineage positive cells: 145-2C11 (CD3ε), GK1.5 (CD4), 53-6.7 (CD8), RB6-8C5 (Ly-6G/Gr1), M1/70 (CD11b/Mac-1), TER119 (Ly-76/TER119), 6B2 (CD45R/B220), and MB19-1 (CD19). The same general procedure of RBC lysis and antibody incubation was used for all other flow cytometry experiments. All antibodies were purchased from BD Pharmingen, eBioscience or BioLegend. All cell sorting and flow cytometry analysis was carried out on a FACSAria III machine (Becton Dickinson) and data were analyzed with FlowJo software (Version 10.7.1).

Immunofluorescence Staining for Mitochondria

The day prior to plating cells, 4-well removable chamber slides (Lab Tek II) were coated with Cell-Tak and kept at 4°C overnight. The next day, FLAG-tag MSCV-MSI2-IRES-GFP or FLAG-tag MSCV-MSI2HOXA9-IRES-GFP infected K562 cells were labeled with 100nM Mitotracker Deep Red FM (Thermo Fisher) at 37°C. After washing twice with PBS, cells were fixed with 4% PFA at 37°C and washed with warm PBS. Cells were spun onto the Cell-Tak coated chamber slides with the brake off and then allowed to settle for an additional 30 minutes. Cells were then permeabilized with 0.1% Triton X-100 for 3 minutes and then blocked in PBS with 10% normal goat serum, 5% bovine serum albumin, 0.3M glycine, and 0.05% Tween-20 for 1 hour. After blocking, cells were incubated with primary antibody in 1:10 diluted blocking buffer overnight at 4°C. The following primary antibodies were used: chicken anti-GFP 1.5:1000 (Abcam) and rabbit anti-FLAG 1.5:1000 (Cell Signaling Technology). Alexa fluor-conjugated secondary antibody (1:500) incubation was performed

for 1 hour at room temperature. DAPI (4-6-diamindino-2-phenylindole; Molecular Probes) was used to detect DNA. Images were obtained with a Zeiss LSM-700 confocal microscope.

Giemsa & May-Grunwald Staining

Lin- cancer was sorted from transplanted mice and spun onto cytospin slides. Slides were allowed to air dry over night before staining with May-Grunwald (Sigma) and Giemsa (diluted 1:20 with DI H_2O, Sigma) stains and again allowed to air dry overnight. Imaging was done using the Keyence BZX-700 fluorescent microscope.

Retroviral Constructs and Production

MIG-BCR-ABL was provided by Warren Pear and Ann Marie Pendergast and was cloned into the MSCV-IRES-NGFR retroviral vector. MSCV-NUP98-HOXA9-IRES-YFP was provided by Gary Gilliland and was sub-cloned into the MSCV-IRES- huCD2 vector (or MSCV-IRES-GFP) retroviral vector. Virus was produced in 293T cells transfected using X-tremeGENE HP (Roche) with viral constructs along with VSV-G and gag-pol. Viral supernatants were collected for three days followed by ultracentrifugal concentration at 20,000x g for 2hr.

qRT-PCR Analysis

RNA was isolated using RNeasy micro kit (Qiagen) and RNA was converted to cDNA using Superscript III reverse transcriptase (Life Technologies). Quantitative realtime PCRs were performed using an iCycler (BioRad) by mixing cDNAs, iQ SYBRGreen Supermix (BioRad) and gene specific primers. Gene expression was normalized to the levels of Beta-2 microglobulin (B2M). All primers were designed using NCBI's Primer-BLAST (https://www.ncbi.nlm.nih.gov/tools/primer-blast/). Primer sequences are listed in Supplementary Table 2.

YSI Bioanalyzer Assay

Lin- leukemic cells were sorted from mice transplanted with BCR-ABL/Control or BCR-ABL/MSI2-HOXA9 transduced KLS cells. Sorted cells were plated in round bottom plates in X-Vivo15 media (Lonza) supplemented with 50 μM 2-mercaptoethanol, 10% (vol/vol) fetal bovine serum (FBS), 1% penicillin-streptomycin, SCF (100 ng/ml, R&D Systems) and TPO (20 ng/ml, R&D Systems). The media supernatant was collected on days 1, 2, and 3 and cell counts were obtained by Trypan Blue counting on days 1 and 3. Glucose, glutamine, glutamate, and lactate concentration in the collected supernatant was measured using a YSI 2950 metabolite analyzer.

Seahorse Assay

The day prior to running the assay, the wells of a XFp plate were coated with Cell-Tak and the plate was kept at 4°C overnight. Lin- leukemic cells were sorted from mice transplanted with BCR-ABL/Control or BCR-ABL/MSI2-HOXA9 transduced KLS cells. Sorted cells were washed twice with complete assay media: XF-DMEM pH 7.4, 1 mM pyruvate, 2 mM L-glutamine, and 10 mM D-glucose. The cells were then aliquoted, spun down, resuspended in 50 uL complete assay media, and added to the previously coated XFp plate. The XFp plate was then spun at 300g for 1 min with the brake off and cell sedimentation was observed by microscope before loading onto the Seahorse XFp analyzer.

RNA Isolation and RNA-seq Analysis

Lin- leukemic cells were sorted from mice transplanted with BCR-ABL/Control or BCR-ABL/MSI2-HOXA9 transduced KLS cells. Total RNA was isolated using the RNeasy Micro Plus kit (QIAGEN). RNA libraries were generated from 150 ng of RNA using Illumina's TruSeq Stranded mRNA Sample Prep Kit (Illumina). Libraries were pooled and single end sequenced (1x75) on the Illumina NextSeq 500 using the High output V2 kit (Illumina).

BCR-ABL/Control and BCR-ABL/MSI2-HOXA9 fastq files were processed into transcript-level summaries using kallisto[31]. Transcript-level summaries were processed into gene-level summaries and differential gene expression was performed using sleuth with the Wald test[32]. GSEA was performed as previously described[33]. ClueGO was used for gene enrichment analysis of all differentially expressed genes (FDR <0.05) identified between BCR-ABL/Control and BCR-ABL/MSI2-HOXA9 mouse cells. GO and Reactome gene sets were used with medium network specificity, a p-value cutoff of <0.05 and a kappa score of 0.4. All other statistical parameters remained on default settings. CluePedia was used to identify genes found within enriched gene sets. All network analyses ran and visualized in Cytoscape 3.7 (Cytoscape, ClueGO/CluePedia).

Statistics and Reproducibility

Statistical analyses were carried out using GraphPad Prism software version 9.2 (GraphPad software Inc.). All data are shown as mean ± SEM. Two-tailed unpaired Student's t-tests were used to determine statistical significance. No statistical method was used to predetermine sample size and no data were excluded from the analysis. All experiments were reproducible.

Data Availability

Primer information is provided in Supplementary Table 2. Antibody information is provided in Supplementary Table 3. Source data are provided with this paper as a separate Source Data file (Supplementary Table 4). Examples of flow cytometry gating strategies are provided as Fig. S3. RNAseq data sets have been deposited into the NCBI GEO database under the accession code GSE159148 and are available through the following

link: https://www.ncbi.nlm.nih.gov/geo/query/acc.cgi?acc=GSE159148. All other data supporting the findings of this study are available within the article and its supplementary information files and from the corresponding author upon reasonable request.

ACKNOWLEDGEMENTS

We would like to thank Warren Pear and Ann Marie Pendergast for providing MIG-BCR-ABL and Gary Gilliland for providing MSCV-NUP98-HOXA9-IRES-YFP. We would also like to thank the Sanford Burnham Prebys Cancer Metabolism Core and Dr. David Scott for their advice and contributions to the work, as well as the University of California San Diego Microscopy Core, which is supported by NIH grant NS047101.

K.S. received support from NIH grants T32 CA009523 and T32 HL086344. M.H. received support from T32 HL086344. J.B. was supported by a postdoctoral fellowship from the National Cancer Center and an ASH Scholar Award. E.D. received support from T32 GM007752. This work was supported by NIH grant R35 CA197699 to T.R.

Author Contributions

K.S. designed and performed experiments and helped write the paper; M.H. performed bioinformatics analysis related to RNAseq and network analysis; J.B., Y.S., E.D. provided experimental advice and support: M.K. helped write the paper; T.R. conceived the project, planned and guided the research and wrote the paper.

COMPETING INTERESTS

T.R. is a founder, and member of the Board of Directors, and holds executive roles at Tiger Hill Therapeutics.

REFERENCES

1 Shah, N. P., Nicoll, J. M., Nagar, B., Gorre, M. E., Paquette, R. L., Kuriyan, J. & Sawyers, C. L. 2002. Multiple BCR-ABL kinase domain mutations confer polyclonal resistance to the tyrosine kinase inhibitor imatinib (STI571) in chronic phase and blast crisis chronic myeloid leukemia. *Cancer Cell* **2**: 117-125.

2 Deininger, M. W., Goldman, J. M. & Melo, J. V. 2000. The molecular biology of chronic myeloid leukemia. *Blood* **96**: 3343-3356.

3 Ahuja, H. G., Popplewell, L., Tcheurekdjian, L. & Slovak, M. L. 2001. NUP98 gene rearrangements and the clonal evolution of chronic myelogenous leukemia. *Genes Chromosomes Cancer* **30**: 410-415.

4 Johansson, B., Fioretos, T. & Mitelman, F. 2002. Cytogenetic and molecular genetic evolution of chronic myeloid leukemia. *Acta Haematol* **107**: 76-94.

5 Mayotte, N., Roy, D. C., Yao, J., Kroon, E. & Sauvageau, G. 2002. Oncogenic interaction between BCR-ABL and NUP98-HOXA9 demonstrated by the use of an in vitro purging culture system. *Blood* **100**: 4177-4184.

6 Yamamoto, K., Nakamura, Y., Saito, K. & Furusawa, S. 2000. Expression of the NUP98/HOXA9 fusion transcript in the blast crisis of Philadelphia chromosome-positive chronic myelogenous leukaemia with t(7;11)(p15;p15). *Br J Haematol* **109**: 423-426.

7 Dash, A. B., Williams, I. R., Kutok, J. L., Tomasson, M. H., Anastasiadou, E., Lindahl, K., Li, S., Van Etten, R. A., Borrow, J., Housman, D., Druker, B. & Gilliland, D. G. 2002. A murine model of CML blast crisis induced by cooperation between BCR/ABL and NUP98/HOXA9. *Proc Natl Acad Sci U S A* **99**: 7622-7627. PMC124303.

8 Kawakami, K., Miyanishi, S., Nishii, K., Usui, E., Murata, T., Shinsato, I. & Shiku, H. 2002. A case of acute myeloid leukemia with t(7;11)(p15;p15) mimicking myeloid crisis of chronic myelogenous leukemia. *Int J Hematol* **76**: 80-83.

9 Barbouti, A., Höglund, M., Johansson, B., Lassen, C., Nilsson, P. G., Hagemeijer, A., Mitelman, F. & Fioretos, T. 2003. A novel gene, MSI2, encoding a putative RNA-binding protein is recurrently rearranged at disease progression of chronic myeloid leukemia and forms a fusion gene with HOXA9 as a result of the cryptic t(7;17)(p15;q23). *Cancer Res* **63**: 1202-1206.

10 Sakakibara, S., Imai, T., Hamaguchi, K., Okabe, M., Aruga, J., Nakajima, K., Yasutomi, D., Nagata, T., Kurihara, Y., Uesugi, S., Miyata, T., Ogawa, M., Mikoshiba, K. & Okano, H. 1996. Mouse-Musashi-1, a neural RNA-binding protein highly enriched in the mammalian CNS stem cell. *Dev Biol* **176**: 230-242.

11 Imai, T., Tokunaga, A., Yoshida, T., Hashimoto, M., Mikoshiba, K., Weinmaster, G., Nakafuku, M. & Okano, H. 2001. The neural RNA-binding protein Musashi1 translationally regulates mammalian numb gene expression by interacting with its mRNA. *Mol Cell Biol* **21**: 3888-3900. PMC87052.

12 Hope, K. J., Cellot, S., Ting, S. B., MacRae, T., Mayotte, N., Iscove, N. N. & Sauvageau, G. 2010. An RNAi screen identifies Msi2 and Prox1 as having opposite roles in the regulation of hematopoietic stem cell activity. *Cell Stem Cell* **7**: 101-113.

13 Nakamura, M., Okano, H., Blendy, J. A. & Montell, C. 1994. Musashi, a neural RNA-binding protein required for Drosophila adult external sensory organ development. *Neuron* **13**: 67-81.

14 Sakakibara, S., Nakamura, Y., Yoshida, T., Shibata, S., Koike, M., Takano, H., Ueda, S., Uchiyama, Y., Noda, T. & Okano, H. 2002. RNA-binding protein Musashi family: roles for CNS stem cells and a subpopulation of ependymal cells revealed by targeted disruption and antisense ablation. *Proc Natl Acad Sci U S A* **99**: 15194-15199. PMC137566.

15 Fox, R. G., Lytle, N. K., Jaquish, D. V., Park, F. D., Ito, T., Bajaj, J., Koechlein, C. S., Zimdahl, B., Yano, M., Kopp, J., Kritzik, M., Sicklick, J., Sander, M., Grandgenett, P. M., Hollingsworth, M. A., Shibata, S., Pizzo, D., Valasek, M., Sasik, R., Scadeng, M., Okano, H., Kim, Y., MacLeod, A. R., Lowy, A. M. & Reya, T. 2016. Image-based detection and targeting of therapy resistance in pancreatic adenocarcinoma. *Nature* **534**: 407-411. PMC4998062.

16 Wang, S., Li, N., Yousefi, M., Nakauka-Ddamba, A., Li, F., Parada, K., Rao, S., Minuesa, G., Katz, Y., Gregory, B. D., Kharas, M. G., Yu, Z. & Lengner, C. J. 2015. Transformation of the intestinal epithelium by the MSI2 RNA-binding protein. *Nat Commun* **6**: 6517. PMC4643281.

17 Ito, T., Kwon, H. Y., Zimdahl, B., Congdon, K. L., Blum, J., Lento, W. E., Zhao, C., Lagoo, A., Gerrard, G., Foroni, L., Goldman, J., Goh, H., Kim, S. H., Kim, D. W., Chuah, C., Oehler, V. G., Radich, J. P., Jordan, C. T. & Reya, T. 2010. Regulation of myeloid leukaemia by the cell-fate determinant Musashi. *Nature* **466**: 765-768. PMC2918284.

18 Kwon, H. Y., Bajaj, J., Ito, T., Blevins, A., Konuma, T., Weeks, J., Lytle, N. K., Koechlein, C. S., Rizzieri, D., Chuah, C., Oehler, V. G., Sasik, R., Hardiman, G. & Reya, T. 2015. Tetraspanin 3 Is Required for the Development and Propagation of Acute Myelogenous Leukemia. *Cell Stem Cell* **17**: 152-164. PMC4664079.

19 Kharas, M. G., Lengner, C. J., Al-Shahrour, F., Bullinger, L., Ball, B., Zaidi, S., Morgan, K., Tam, W., Paktinat, M., Okabe, R., Gozo, M., Einhorn, W., Lane, S. W., Scholl, C., Fröhling, S., Fleming, M., Ebert, B. L., Gilliland, D. G., Jaenisch, R. & Daley, G. Q. 2010. Musashi-2 regulates normal hematopoiesis and promotes aggressive myeloid leukemia. *Nat Med* **16**: 903-908. PMC3090658.

20 Makhov, P., Bychkov, I., Faezov, B., Deneka, A., Kudinov, A., Nicolas, E., Brebion, R., Avril, E., Cai, K. Q., Kharin, L. V., Voloshin, M., Frantsiyants, E., Karnaukhov, N., Kit, O. I., Topchu, I., Fazliyeva, R., Nikonova, A. S., Serebriiskii, I. G., Borghaei, H., Edelman, M., Dulaimi, E., Golemis, E. A. &

Boumber, Y. 2021. Musashi-2 (MSI2) regulates epidermal growth factor receptor (EGFR) expression and response to EGFR inhibitors in EGFR-mutated non-small cell lung cancer (NSCLC). *Oncogenesis* **10**: 29. PMC7961039.

21 Ohyama, T., Nagata, T., Tsuda, K., Kobayashi, N., Imai, T., Okano, H., Yamazaki, T. & Katahira, M. 2012. Structure of Musashi1 in a complex with target RNA: the role of aromatic stacking interactions. *Nucleic Acids Res* **40**: 3218-3231. PMC3326303.

22 Chance, B. & Williams, G. R. 1955. Respiratory enzymes in oxidative phosphorylation. III. The steady state. *J Biol Chem* **217**: 409-427.

23 Yehudai, D., Liyanage, S. U., Hurren, R., Rizoska, B., Albertella, M., Gronda, M., Jeyaraju, D. V., Wang, X., Barghout, S. H., MacLean, N., Siriwardena, T. P., Jitkova, Y., Targett-Adams, P. & Schimmer, A. D. 2019. The thymidine dideoxynucleoside analog, alovudine, inhibits the mitochondrial DNA polymerase γ, impairs oxidative phosphorylation and promotes monocytic differentiation in acute myeloid leukemia. *Haematologica* **104**: 963-972. PMC6518883.

24 Zhao, F., Sun, L., Yang, N., Zheng, W., Shen, P., Huang, Y. & Lu, Y. 2020. Increased release of microvesicles containing mitochondria is associated with the myeloid differentiation of AML-M5 leukaemia cells. *Exp Cell Res* **395**: 112213.

25 Wang, K., Sanchez-Martin, M., Wang, X., Knapp, K. M., Koche, R., Vu, L., Nahas, M. K., He, J., Hadler, M., Stein, E. M., Tallman, M. S., Donahue, A. L., Frampton, G. M., Lipson, D., Roels, S., Stephens, P. J., Sanford, E. M., Brennan, T., Otto, G. A., Yelensky, R., Miller, V. A., Kharas, M. G., Levine, R. L., Ferrando, A., Armstrong, S. A. & Krivtsov, A. V. 2017. Patient-derived xenotransplants can recapitulate the genetic driver landscape of acute leukemias. *Leukemia* **31**: 151-158. PMC5203983.

26 De Weer, A., Speleman, F., Cauwelier, B., Van Roy, N., Yigit, N., Verhasselt, B., De Moerloose, B., Benoit, Y., Noens, L., Selleslag, D., Lippert, E., Struski, S., Bastard, C., De Paepe, A., Vandenberghe, P., Hagemeijer, A., Dastugue, N. & Poppe, B. 2008. EVI1 overexpression in t(3;17) positive myeloid malignancies results from juxtaposition of EVI1 to the MSI2 locus at 17q22. *Haematologica* **93**: 1903-1907.

27 Saleki, R., Christensen, T., Liu, W., Wang, X., Chen, Q. C., Aakre, M., Gomes, N. M., Alexiev, B. A., Schappert, J., Baer, M. R. & Zou, Y. S. 2015. A novel TTC40-MSI2 fusion in de novo acute myeloid leukemia with an unbalanced 10;17 translocation. *Leuk Lymphoma* **56**: 1137-1139. PMC4589160.

28 Jang, Y.E., Jang, I., Kim, S., Cho, S., Kim, D., Kim, K., Kim, J., Hwang, J., Kim, S., Kim, J., Kang, J., Lee, B., Lee, S. ChimerDB 4.0: an updated and expanded database of fusion genes. *Nucleic Acids Res* **48**: D817-D824. PMC7145594.

29 Zimdahl, B., Ito, T., Blevins, A., Bajaj, J., Konuma, T., Weeks, J., Koechlein, C. S., Kwon, H. Y., Arami, O., Rizzieri, D., Broome, H. E., Chuah, C., Oehler, V. G., Sasik, R., Hardiman, G. & Reya, T.

2014. Lis1 regulates asymmetric division in hematopoietic stem cells and in leukemia. *Nat Genet* **46**: 245-252. PMC4267534.

30 Domen, J., Cheshier, S. H. & Weissman, I. L. 2000. The role of apoptosis in the regulation of hematopoietic stem cells: Overexpression of Bcl-2 increases both their number and repopulation potential. *J Exp Med* **191**: 253-264. PMC2195763.

31 Bray, N. L., Pimentel, H., Melsted, P. & Pachter, L. 2016. Near-optimal probabilistic RNA-seq quantification. *Nat Biotechnol* **34**: 525-527.

32 Pimentel, H., Bray, N. L., Puente, S., Melsted, P. & Pachter, L. 2017. Differential analysis of RNA-seq incorporating quantification uncertainty. *Nat Methods* **14**: 687-690.

33 Lytle, N. K., Ferguson, L. P., Rajbhandari, N., Gilroy, K., Fox, R. G., Deshpande, A., Schürch, C. M., Hamilton, M., Robertson, N., Lin, W., Noel, P., Wartenberg, M., Zlobec, I., Eichmann, M., Galván, J. A., Karamitopoulou, E., Gilderman, T., Esparza, L. A., Shima, Y., Spahn, P., French, R., Lewis, N. E., Fisch, K. M., Sasik, R., Rosenthal, S. B., Kritzik, M., Von Hoff, D., Han, H., Ideker, T., Deshpande, A. J., Lowy, A. M., Adams, P. D. & Reya, T. 2019. A Multiscale Map of the Stem Cell State in Pancreatic Adenocarcinoma. *Cell* **177**: 572-586.e522. PMC6711371.

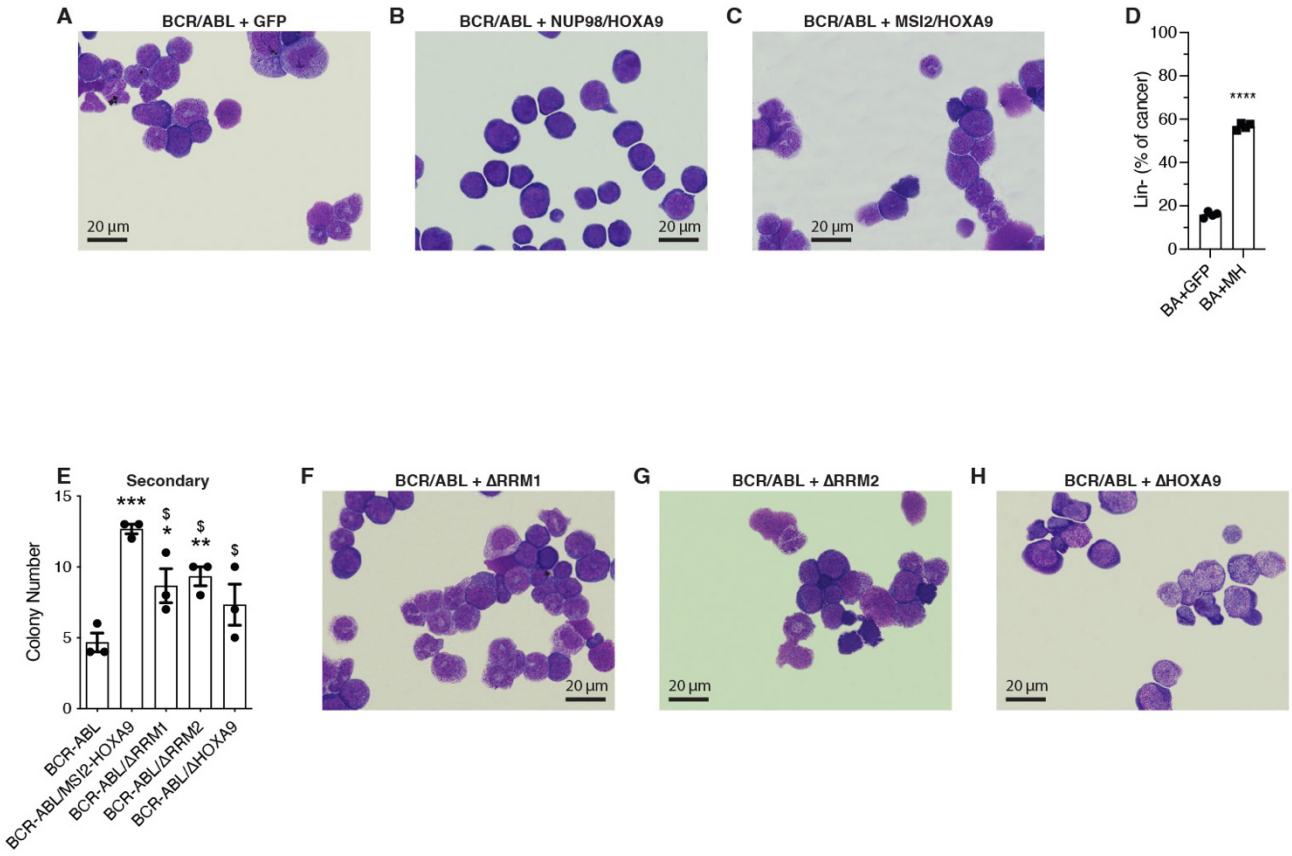

Figure S1. Analysis of BCR-ABL/MSI2-HOXA9 leukemia

(*A-C*) Representative brightfield image of (*A*) BCR-ABL/Control, (*B*) BCR-ABL/NUP98-HOXA9, (*C*) BCR-ABL/MSI2-HOXA9 cytospins of lin- cancer stained with Giemsa and May-Grunwald stains. (*D*) Quantification of BCR-ABL/MSI2-HOXA9 and BCR-ABL Lin- content within the cancer population by FACS. ****P<0.0001, n=4 for each group. (*E*) Secondary colony formation of KLS cells expressing BCR-ABL/Control or BCR-ABL + variations of the MSI2-HOXA9 fusion protein. *=significance from BCR-ABL/Control, *P=0.04, **P=0.007 ***P=0.0004; $=significance from BCR-ABL/MSI2-HOXA9, $P=0.03 for ΔRRM1, $P=0.01 for ΔRRM2, $P=0.02 ΔHOXA9 (n=3 technical replicates). (*F-H*) Representative brightfield image of (*F*) BCR-ABL/ΔRRM1, (*G*) BCR-ABL/ΔRRM2 (*H*) BCR-ABL/ΔHOXA9 cytospins of lin- cancer stained with Giemsa and May-Grunwald stains.

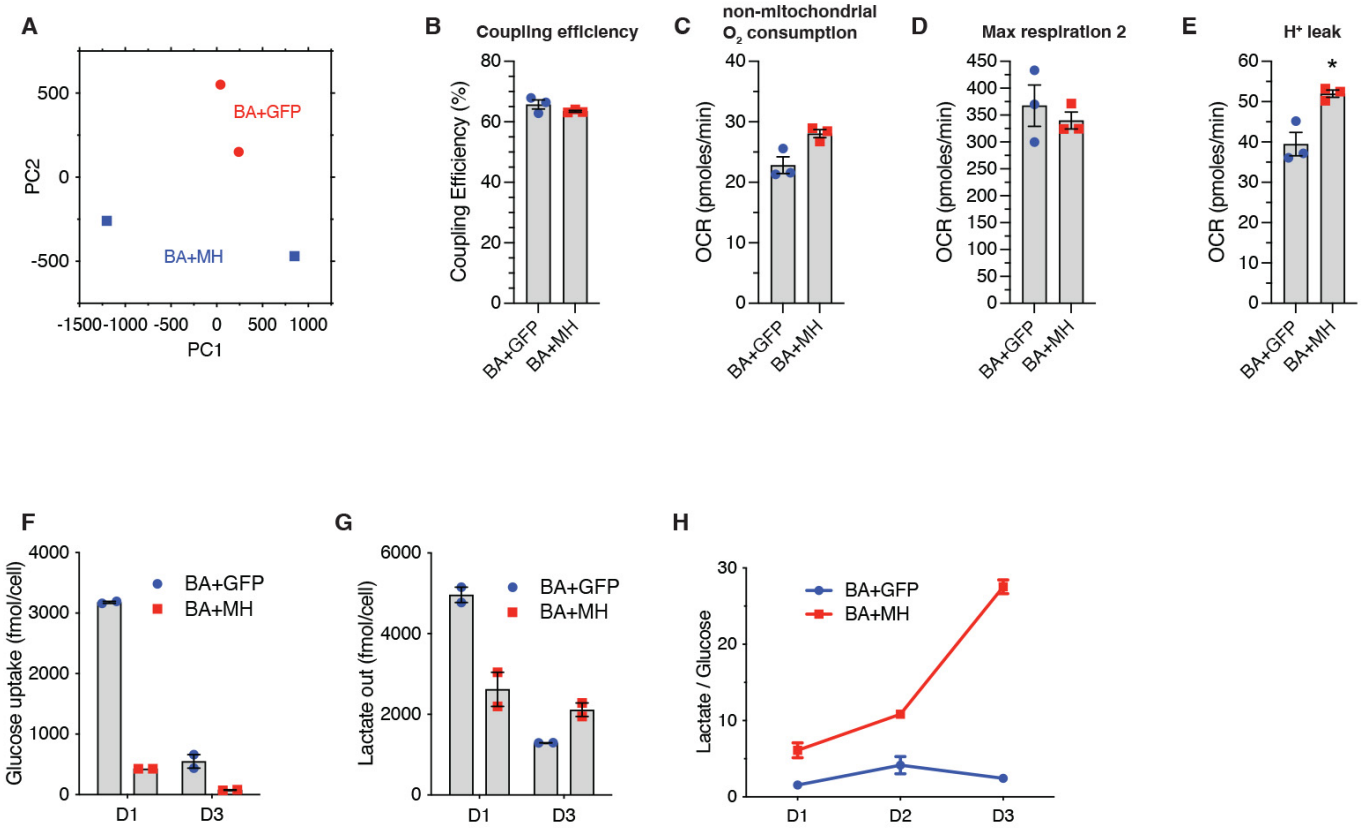

Figure S2. Principal component analysis and mitochondrial parameters associated with BCR-ABL/MSI2-HOXA9 leukemia

(*A*) Principal component analysis of RNAseq data of Lin- BCR-ABL/Control and Lin- BCR-ABL/MSI2-HOXA9. (*B*) Coupling efficiency determined from OCR of Lin- BCR-ABL/Control and Lin- BCR-ABL/MSI2-HOXA9 (n=3 technical replicates). (*C*) Non-mitochondrial O_2 consumption determined from OCR of Lin- BCR-ABL/Control and Lin- BCR-ABL/MSI2-HOXA9 (n=3 technical replicates). (*D*) Maximum respiration determined from OCR of Lin- BCR-ABL/Control and Lin- BCR-ABL/MSI2-HOXA9 following the second FCCP injection, an oversaturating concentration (n=3 technical replicates). (*E*) Proton leak determined from OCR of Lin- BCR-ABL/Control and Lin- BCR-ABL/MSI2-HOXA9. *P=0.01 (n=3 technical replicates). (*F*) Glucose uptake of Lin- BCR-ABL/Control and Lin- BCR-ABL/MSI2-HOXA9 measured by the YSI bioanalyzer at day 1 (D1) and day 3 (D3) post-plating (n=2 technical replicates). (*G*) Lactate production of Lin- BCR-ABL/Control and Lin- BCR-ABL/MSI2-HOXA9 measured by the YSI bioanalyzer at day 1 (D1) and day 3 (D3) post-plating (n=2 technical replicates). (*H*) Ratio of lactate production to glucose consumption of Lin- BCR-ABL/Control and Lin- BCR-ABL/MSI2-HOXA9 at day 1 (D1), day 2 (D2), and day 3 (D3) post-plating (n=2 technical replicates).

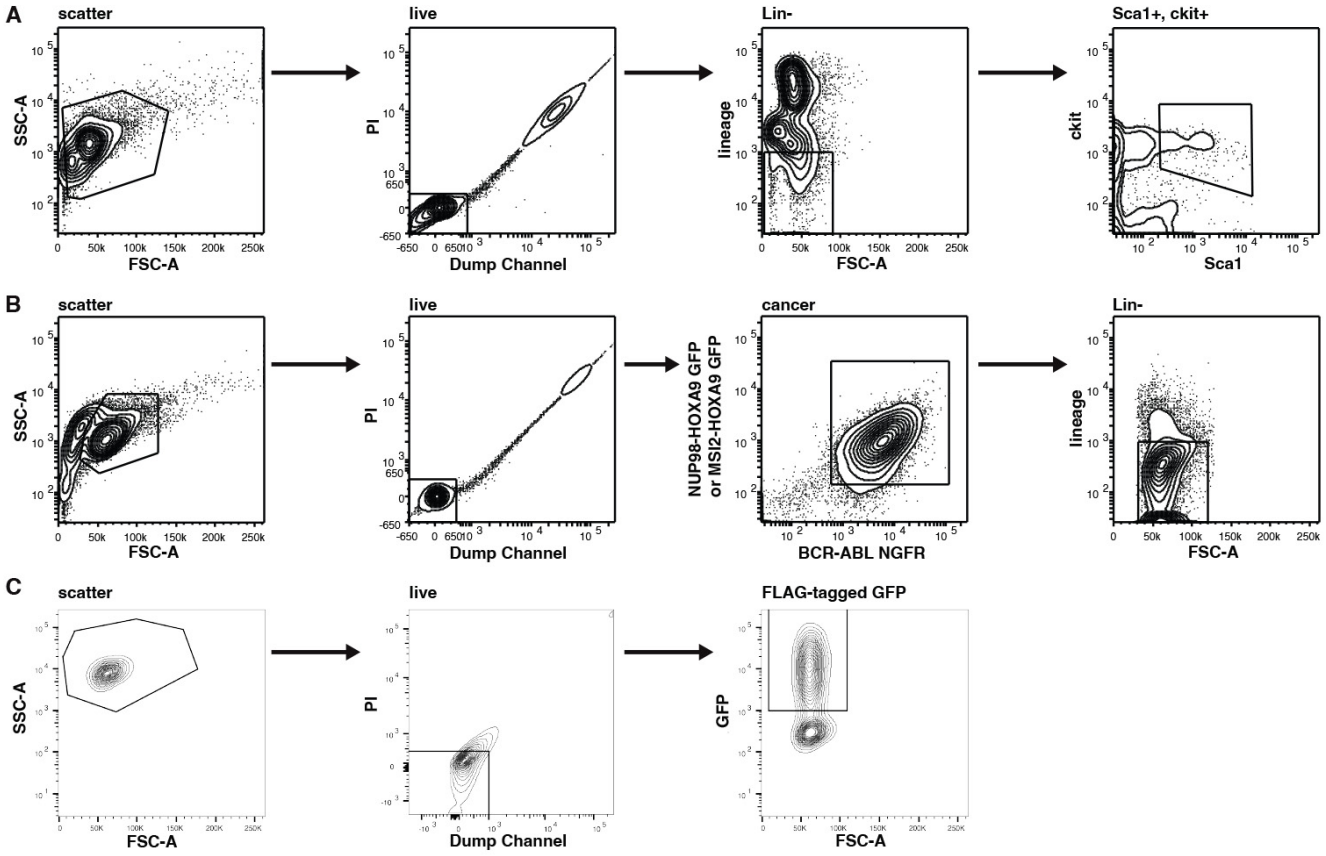

Figure S3. Examples of flow cytometry gating strategies

(*A*) Gating strategy used for KLS sorting from mouse bone marrow. KLS cells were used as starting material for all mouse leukemia models in this paper. (*B*) Gating strategy used for sorting lin- bcCML from primary transplants. This strategy was used to generate the cell source for histology, transplants, and RNAseq. (*C*) Gating strategy used for isolating FLAG-tagged transduced K562 cells. After 48hrs in the presence of BCR-ABL + FLAG-tagged wild-type MSI2 or FLAG-tagged MSI2/HOXA9, cells were sorted to isolate doubly infected cells. This strategy was used for the localization experiments (Fig. 5B-D).